Lossy Microwave Filters With Active Shape Correction

GOKHAN ARITURK[1,2], **(Graduate Student Member, IEEE),**
AND HJALTI H. SIGMARSSON[1,2], **(Senior Member, IEEE)**
[1]Advanced Radar Research Center, The University of Oklahoma, Norman, OK 73019, USA
[2]School of Electrical and Computer Engineering, The University of Oklahoma, Norman, OK 73019, USA

Corresponding author: Gokhan Ariturk (gokhan.ariturk@ou.edu)

ABSTRACT Obtaining the prescribed microwave filter response is highly desirable for proper frequency selectivity in RF transceivers. As the traditional microwave filter design methods do not take into account finite unloaded quality factors, lossy resonators cause significant deviations from the prescribed filter response, especially in filters with narrow bandwidths or of high orders. This deviation gets more severe as the resonator losses increase. Building on the lossy filter design techniques by using an active shape correction mechanism, this paper proposes a new approach to recover the filter response when the filter has moderately-to-highly lossy resonators. Being different than most active filter topologies, where all of the resonators are loss-compensated, this study aims at achieving the shape correction with $N - 2$ active elements. To characterize the design, a novel *lossy-active coupling matrix* is introduced by extending the $(N + 2) \times (N + 2)$ lossy coupling matrix. The proposed theory is verified with the design and fabrication of two 3rd order 5 % bandwidth filters operating at 1 GHz and employing resonators with quality factors of 100 and 28, respectively. It has been shown that the method can recover the response in both designs and the theoretical and measured responses are in good agreement.

I. INTRODUCTION

Analog microwave filters are among the most important components of the front-end modules of radio frequency (RF) transceivers. As the filter response significantly affects the overall transceiver performance, obtaining the ideal (prescribed) response is highly desirable.

The most common method of designing a bandpass filter is to use the *g*-coefficients for a lowpass prototype and have a lowpass-to-bandpass conversion [1], [2]. This method assumes that the filter resonators are lossless and makes it possible to obtain almost any desired filter response. As filters are miniaturized, the reduced resonator quality factors (Q) cause the filter shape to be perturbed, which makes it difficult to design narrow-band and/or higher-order filters with resonators of low-Q. The shape perturbation is tolerable for microstrip-, cavity-, or dielectric-resonator-based filters,

especially when the filter order is low. However, it causes significant selectivity and overall shape degradations when lumped element resonators are used, such as in monolithic microwave integrated circuit (MMIC) based filters.

To overcome the effects of finite-Q and electronically perform loss compensation, various topologies of active microwave filters have been proposed. In [3]–[6], coupled negative resistance approach with field-effect transistors (FET) are used. To have a negative resistance effect, parametric amplification is used for loss compensation in [7] and a further coupling manipulation is used for shape and selectivity enhancement in [8] for narrow-band filter realization.

As the major origin of the loss is identified as the lumped inductors, the concept of active inductor design for narrow-band MMIC filter applications was performed with FET transistors in [9] and [10] and with the inverted collector technique based bipolar transistors in [11] and [12]. Furthermore, dynamic range and nonlinearity considerations of active inductors were presented in [13] and [14]. In [15]–[17],

The associate editor coordinating the review of this manuscript and approving it for publication was Andrei Muller.

GaAs FETs are used to link the resonant structures to not only compensate for the loss, but to produce gain within the passband. Finally, the transversal active MMIC filter topology is used in [18] and [19] to improve the shape of the response.

A different technique to recover the filter response is the design of lossy filters [20]–[31]. In its essence, the concept is based on correcting the filter response and selectivity by accepting additional insertion loss (IL) within the passband. This technique was initially proposed in [20] as the classical method of predistortion, where the design is based on shifting the poles of the transfer function (S_{21}) on the complex plane to account for the losses. It was further enhanced in [21] by distributing the loss among the resonators using hyperbolic rotations and resistive cross-coupling among non-adjacent nodes. Two other examples that include filters with non-uniform dissipation are given in [22], [23].

Within the context of lossy filters, the *lossy coupling matrix* is introduced in [25]–[27]. In [25], the lossy filter is characterized as a lossless filter with an input and an output attenuator. The lossy coupling matrix is constructed by transferring the series resistances within the lumped element model of the attenuators towards the filter resonators. Drawing on that idea, the generalized lossy $N \times N$ and the transversal $(N + 2) \times (N + 2)$ coupling matrices (N being the filter order) are introduced in [26] and [27], respectively. In [26], the complex coupling matrix is synthesized from the lossy Chebyshev polynomials by considering its diagonalizability to its eigenvalue matrix. Following that, the transversal lossy coupling matrix is generated directly from the lossy admittance polynomials by using their residues in [27].

To distribute the losses evenly among the resonators or to manipulate the routing topology of lossy filters, hyperbolic rotations are used in [26] and [27]. In that regard, performance metrics of inline and transversal lossy filter structures are compared in [28] and loss equalization methods are proposed in [30] and [32]. The hyperbolic matrix rotations produce purely imaginary and/or complex inter-resonator coupling mechanisms, which pose a challenge in terms of the practical implementation of lossy filters. While that issue is briefly addressed in [26], a more exact passive realization method based on resistive decomposition of the lossy coupling mechanisms is presented in [32].

Based on waveguide filter-amplifier co-design techniques, [33] proposes an $(N + 3) \times (N + 3)$ *active coupling matrix* for an X-band second-order filter-amplifier cascade. In [33], the inter-resonator coupling values were calculated using the g-coefficients while the additional entries due to the cascaded amplifier were found from the admittance matrix of the small-signal model of an FET. A more comprehensive $(N + 4) \times (N + 4)$ active coupling matrix was proposed in [34], where the amplifier network was included within the inter-resonator path, linking noise figure (NF) and the coupling matrix. The lossy design approaches discussed so far are proposed for macro-scale filters where the resonators have moderate-to-high quality factors ($Q_u > 100$).

In the current study, a new approach of using active resonators within the concept of lossy filter design is presented. The objective is to recover the filter shape in the presence of moderate to highly lossy resonators. Unlike the common active filter approaches, where all the resonators are loss-compensated, the proposed design uses $N - 2$ active elements for the shape correction. Furthermore, the lossy coupling matrix in [25] is extended to propose the novel *lossy-active coupling matrix* for the first time. To prove the concept, two third-order 20 dB equiripple 5% fractional bandwidth (FBW) filters with different loss levels are designed and implemented. The first design recovers the shape of the filter with a Q_u of 100 at each resonator, whereas the second prototype, illustrating the use of highly lossy resonators, recovers the response at a Q_u of 28 at each resonator.

II. THEORY

Drawing upon complex coupling matrix theory, this section begins with the design of an inline passive lossy filter structure that includes resonators with non-uniform quality factor distribution. Proceeding with the design, integration of the active element is explained and the design of an Nth order lossy-active filter is presented. To characterize the design, the *lossy-active coupling matrix* is introduced. The concept is illustrated with a third-order 20-dB equiripple (when lossless) filter with 5% fractional bandwidth.
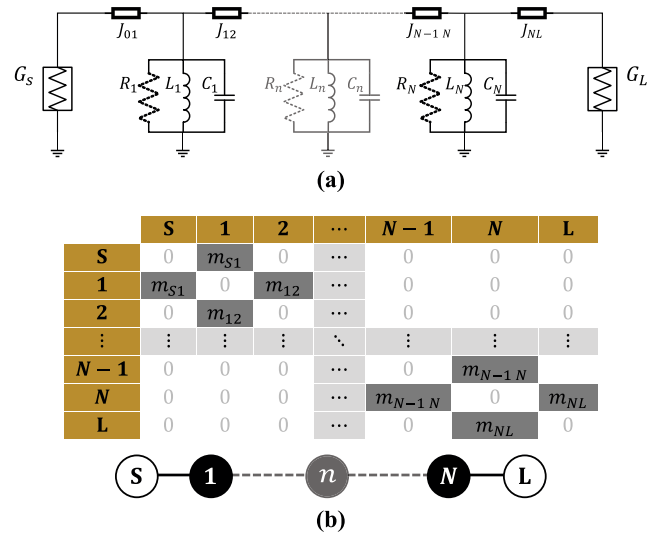

FIGURE 1. (a): Schematic of a conventional bandpass filter of order N with the inclusion of loss as shunt resistors. (b): The lossless $(N + 2) \times (N + 2)$ coupling matrix and the coupling diagram.

A. LOSSY FILTER DESIGN

Using conventional filter design procedure, Fig. 1 (a) depicts an Nth−order bandpass filter structure. As observed, L_n is the equivalent inductance and C_n is the equivalent capacitance of the nth parallel resonator, resonating at a center frequency of $\omega_0 = 1/(\sqrt{L_n C_n})$. Representing the loss in each resonator, shunt resistors are shown as the dashed lines, labeled as R_n. The admittance inverters that produce the coupling between

the nth and m^{th} resonator are denoted as J_{nm}, such that $n, m \in \{1, 2, \ldots, N\}$ and the input and output inverters are denoted as J_{S1} and J_{NL}, respectively. Characterizing the lossless filter, i.e., $R_n \rightarrow \infty \ \forall n$, the lossless $(N + 2) \times (N + 2)$ coupling matrix and the coupling diagram are depicted in Fig. 1 (b). For this configuration, the coupling matrix entries are calculated as:

$$m_{n,n+1} = \frac{1}{\sqrt{g_n g_{n+1}}} \quad n \in \{1, 2, \ldots, N\},$$

$$m_{s1} = \frac{1}{\sqrt{g_0 g_1}}, \quad m_{NL} = \frac{1}{\sqrt{g_N g_{N+1}}}. \quad (1)$$

The traditional design practices of using the g-coefficients assume that the filter resonators are lossless, just as in the lossless coupling matrix. In practical lossy resonators, the unloaded quality factor of the nth resonator is calculated as $Q_{un} = R_n/(\omega_0 L_n)$. To visualize the effect of the loss, the finite Q_u can be introduced to the coupling matrix by replacing the complex frequency variable s with $s + 1/(FBW \cdot Q_u)$. Here, s is in the form of the bandpass variable such that $s = (j/FBW)(\omega/\omega_0 - \omega_0/\omega)$, where ω is the radian frequency.
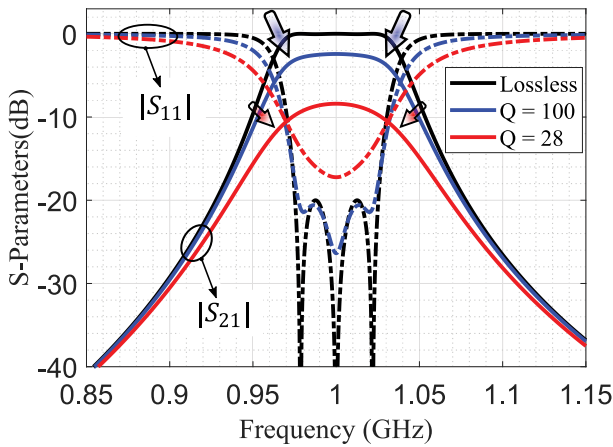

FIGURE 2. Effect of decreasing resonator Q_u on the filter response. S_{11} is plotted with the solid line and S_{21} is plotted with the dashed line. The responses of a 5% FBW 20-dB equiripple design having resonators of infinite Q_u, $Q_u = 100$, and $Q_u = 28$ are depicted.

The reflection ($|S_{11}|$) and the transmission ($|S_{21}|$) responses of a lossless third-order 20-dB equiripple, 5% FBW bandpass filter are depicted in Fig. 2 with the black trace. To show the effect of decreasing Q_u, the figure also depicts the filter responses for two other filters with different resonator quality factor values. It should be pointed out that the resonators in each individual filter have equivalent quality factors, i.e., $R_1 = R_2 = R_3$ and $L_1 = L_2 = L_3$ for each example. As observed, the desired lossless filter response, such that $Q_{u_n} \rightarrow \infty \ \forall n$, has the highest selectivity and the best reflection response. As the Q_u of each resonator is reduced, the transmission response starts to have rounded passband edges and increased return loss at a Q_u of 100 and a completely perturbed selectivity, weak reflection response,
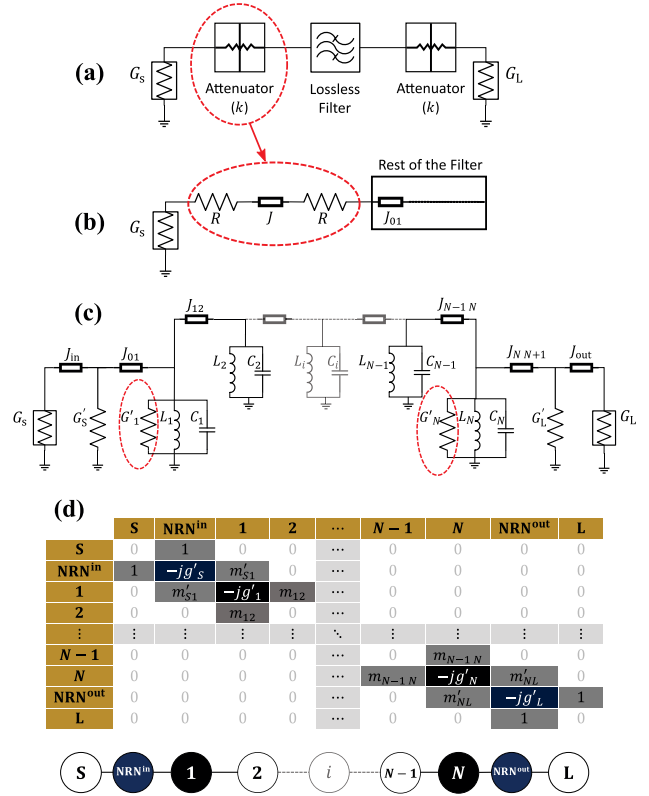

FIGURE 3. (a): The lossy filter model in [25] as a starting point. (b): The resistor-admittance inverter-resistor based model of the attenuators in (a) with an attenuation factor of *k* in linear scale. (c): The synthesized lossy filter including loss in the input and output resonators [25]. (d): The $(N + 2) \times (N + 2)$ lossy coupling matrix and the coupling diagram of the filter in (c). In the coupling matrix and the diagram, *S* denotes the source, *L* denotes the load and *NRN* is for the non-resonating nodes.

and a distorted passband flatness when the Q_u of each resonator is 28.

To correct the shape of the filter response when the resonators have finite quality factors, an Nth order lossy filter is synthesized with the method in [25]. The design is based on the lossy synthesis method emulating the cascade of two attenuators at the input and output of the lossless filter, each of which has an attenuation factor of *k*, as depicted in Fig. 3 (a). The reflection and transmission responses of the lossy filter (S_{11}^{lossy} and S_{21}^{lossy}), are formulated in terms of those of the lossless one as:

$$S_{11}^{lossy} = k^2 S_{11}^{lossless},$$
$$S_{21}^{lossy} = k^2 S_{21}^{lossless}, \quad (2)$$

where *k* is the attenuation factor in linear scale. In (2), the lossless filter responses ($S_{11}^{lossless}$ and $S_{21}^{lossless}$) are characterized by the conventional polynomial synthesis method and are given as in the following [1]:

$$|S_{21}^{lossless}|^2 = 1 - |S_{11}^{lossless}|^2 = \frac{1}{1 + \epsilon^2 |K_N(s)|^2}, \quad (3)$$

where $|K_N(s)|$ is the Nth degree characteristic polynomial of the filter function and ϵ is the ripple factor.

Modeling the input and output attenuators as resistor-admittance inverter-resistor cascade as in Fig. 3 (b), shifting the series resistors towards the filter resonators as shunt conductances, and scaling the input/output inverters to unity as in [25], the circuit in Fig. 3 (c) is obtained. The lossy coupling matrix and the coupling diagram of that filter are depicted in Fig. 3 (d).

To achieve an attenuation factor of k with the attenuator model in Fig. 3 (b), the admittance inverter and the pair of resistors need to have the following relation [25]:

$$J = \pm \frac{1}{\sqrt{1 - R^2}}, \quad k = \sqrt{\frac{1 - R}{1 + R}}, \quad (4)$$

where J is the value of the admittance inverter and R is the value of the resistor pair. The additional entries in the coupling matrix, including the shunt conductances at the non-resonating nodes (g'_S and g'_L) and at the lossy resonators (g'_1 and g'_N), are formulated as in the following:

$$g'_S = g'_L = R = \frac{1 - k^2}{1 + k^2},$$
$$m'_{S1} = \pm m_{S1} \sqrt{1 - R^2}, \quad m'_{NL} = \pm m_{NL} \sqrt{1 - R^2},$$
$$g'_1 = R m^2_{S1}, \quad g'_N = R m^2_{NL}. \quad (5)$$

Considering (4), the initial parameter to be determined in the lossy filter design is the attenuation factor k, as it determines the required unloaded quality factors of the input and output resonators. To obtain the admittance inverter values in Fig. 3 (c) from the coupling matrix entries, the entries need to be scaled according to the source/load resistances, the operating frequency, and the FBW of the bandpass filter. The required quality factors at the input/output resonators depend on the attenuation factor and the operating frequency.

Further observing Fig. 3 (c) and (d), one can realize that there is no loss in the resonators through 2 to $N - 1$. With the use of hyperbolic rotations and resistive cross-coupling among different nodes, the loss could have been uniformly distributed among the resonators of the filter [21], [24], [25], however, that is beyond the scope of this study. Until this point, the resonators through 2 to $N - 1$ are still considered to be lossless.

B. LOSS COMPENSATION IN RESONATORS

The lossless resonators in Fig. 3 (c) have been realized with the use of waveguides, cavities, or dielectric structures to achive high unloaded quality factors, typically greater than 1000 for the microwave frequencies [25]–[27]. However, resonators with those quality factors are not achievable in PCBs or MMICs, therefore in this study, they are realized using active resonators.

In Fig. 4, an active resonator with a coupled feedback amplifier is depicted. The amplifier is coupled to the resonator with the external quality factors of Q_1 and Q_2 through the impedance inverters K_1 and K_2.

The external quality factors Q_1 and Q_2 are dependent on both the impedance inverter values K_1 and K_2 and the
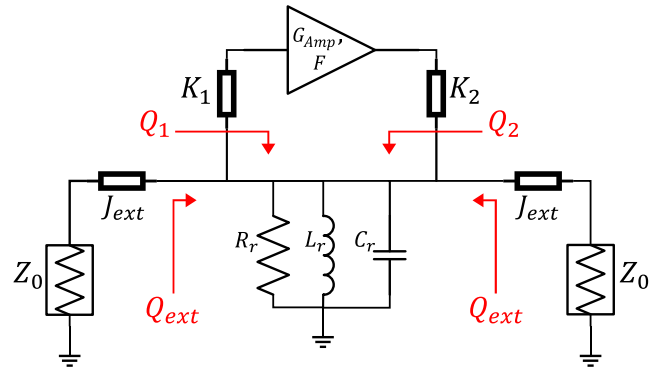
FIGURE 4. Illustration of an active loss compensated resonator.

input/output impedances of the amplifier. Assuming that the input and output impedances of the amplifier are matched to 50 Ω, the external quality factors are given as:

$$Q_1 = \frac{K_1^2}{50 \omega_0 L_r} \quad \text{and} \quad Q_2 = \frac{K_2^2}{50 \omega_0 L_r}. \quad (6)$$

With the external quality factors of the amplifier loop, the effective active negative resistance that is seen at the lossy resonator side can be calculated as [35]:

$$R_{negative} = \left(-\frac{\frac{K_2^2}{50}}{2 G_{Amp} \frac{K_2}{K_1} - 1} \right) \| \left(\frac{K_1^2}{50} \right), \quad (7)$$

where G_{Amp} is the voltage gain of the amplifier in linear scale. As mentioned in [35], the full loss compensation at the lossy resonator is achieved when the negative resistance in (7) has the same magnitude as the resistance of the parallel resonator R_r. That equality will be achieved when the relationship between the amplifier gain (G_{Amp}), the unloaded quality factor of the resonator (Q_{u_r}), and the external quality factors Q_1 and Q_2 have the following relation [35]:

$$G_{Amp} = \frac{\sqrt{Q_1 Q_2}}{2} \cdot \left(Q_{u_r}^{-1} + Q_1^{-1} + Q_2^{-1} \right). \quad (8)$$

In addition to (8), it is important that the phase response of the amplifier feedback loop is an integer multiple of 360° for full loss compensation.

In the loss-compensated resonator, it is highly desirable to minimize the additional noise figure contribution of the active portion. It has also been discussed in [35]–[37] that the minimum noise with an active resonator can be achieved when the following relationship is satisfied:

$$Q_2 = G_{Amp}^2 Q_1. \quad (9)$$

Combining (8) and (9), one can obtain the following relationships between the external quality factors and the amplifier gain:

$$Q_1 = \frac{G_{Amp}^2 - 1}{G_{Amp}^2} Q_{u_r} \quad \text{and} \quad Q_2 = (G_{Amp}^2 - 1) Q_{u_r}. \quad (10)$$

Therefore, it is important to satisfy the relations in (10) to have a fully loss compensated resonator with minimum additional noise figure from the amplifier. This design technique
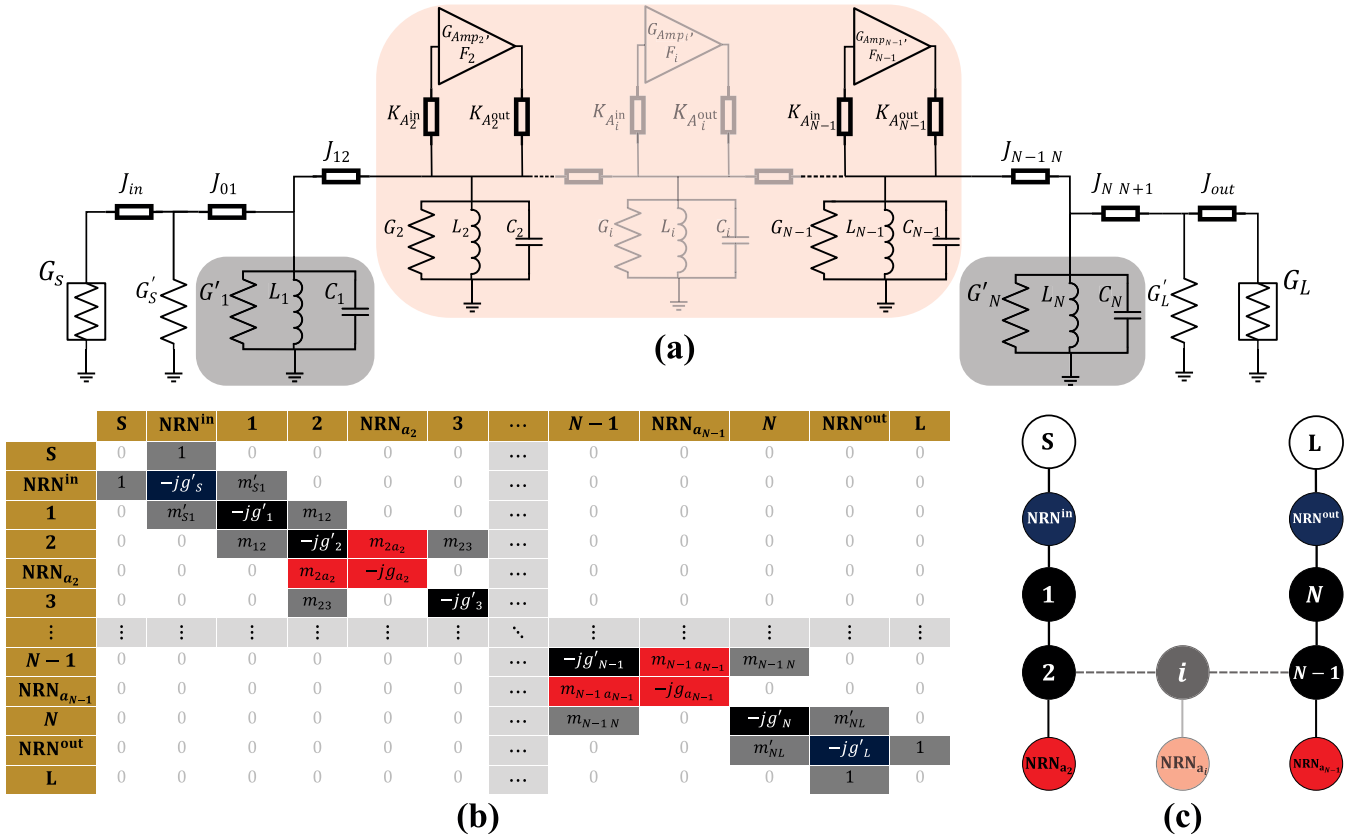
(a)

	S	NRN^{in}	1	2	NRN$_{a_2}$	3	$\cdots$	$N-1$	NRN$_{a_{N-1}}$	N	NRN^{out}	L
S	0	1	0	0	0	0	$\cdots$	0	0	0	0	0
NRN^{in}	1	$-jg'_S$	m'_{S1}	0	0	0	$\cdots$	0	0	0	0	0
1	0	m'_{S1}	$-jg'_1$	m_{12}	0	0	$\cdots$	0	0	0	0	0
2	0	0	m_{12}	$-jg'_2$	m_{2a_2}	m_{23}	$\cdots$	0	0	0	0	0
NRN$_{a_2}$	0	0	0	m_{2a_2}	$-jg_{a_2}$	0	$\cdots$	0	0	0	0	0
3	0	0	0	m_{23}	0	$-jg'_3$	$\cdots$	0	0	0	0	0
$\vdots$	$\vdots$	$\vdots$	$\vdots$	$\vdots$	$\vdots$	$\vdots$	$\ddots$	$\vdots$	$\vdots$	$\vdots$	$\vdots$	$\vdots$
$N-1$	0	0	0	0	0	0	$\cdots$	$-jg'_{N-1}$	$m_{N-1\,a_{N-1}}$	$m_{N-1\,N}$	0	0
NRN$_{a_{N-1}}$	0	0	0	0	0	0	$\cdots$	$m_{N-1\,a_{N-1}}$	$-jg_{a_{N-1}}$	0	0	0
N	0	0	0	0	0	0	$\cdots$	$m_{N-1\,N}$	0	$-jg'_N$	m'_{NL}	0
NRN^{out}	0	0	0	0	0	0	$\cdots$	0	0	m'_{NL}	$-jg'_L$	1
L	0	0	0	0	0	0	$\cdots$	0	0	0	1	0

(b)

(c)

FIGURE 5. (a): The lossy-active filter with loss compensation in the resonators 2 through $N-1$. (b): The lossy-active coupling matrix that characterizes the network in (a). (c): The routing diagram of the filter. NRN^{in} and NRN^{out} represent the non-resonant nodes at the input and output. NRN$_{a_i}$ denotes the ith amplifier loop as a single non-resonating node that acts like a negative resistance.

provides the flexibility of using resonators with arbitrary unloaded quality factors to start with as long as the impedance inverters providing the external quality factors (Q_1 and Q_2) are realizable. For convenience, the resonators 2 through $N-1$ are chosen to be identical to the first and the last resonator of the filter in this study.

Apart from the input and output coupling of the amplifier (K_1 and K_2), the NF of the active resonator stage is determined by several factors. These include the external quality factors that are introduced to the resonator, the gain of the feedback amplifier, and most importantly, the unloaded quality factor of the passive resonator. Considering that the relations in (10) are satisfied for the active resonator in Fig. 4, the minimum noise figure of the resonator stage is given by [35], [37]:

$$F_{min} = F_{passive} + \frac{Q_e}{Q_u}M,$$

where

$$M = \left(\frac{F-1}{1-\frac{1}{G_{Amp}^2}}\right) \text{ and } F_{passive} = 1 + \frac{Q_e}{2Q_u}. \quad (11)$$

In (11), M is the noise measure of the amplifier [35] and $F_{passive}$ is the NF of the passive resonator when the amplifier

network (including K_1 and K_2) is not connected. A fundamental observation regarding (11) is that the noise figure of the active resonator has to be greater than $F_{passive}$ and it is highly dependent on the noise measure of the amplifier. The effect of slight variations of K_1, K_2, and the noise measure on the noise figure of the resonator was thoroughly discussed in [35]. It is important to emphasize that the noise figure given by (11) is the noise figure of the single active resonator and not the overall filter. The effect of the noise figure of active resonators on the entire filter is dependent on different factors including the order of the resonators and the placement of the active resonator among them. Those factors were discussed and a noise figure estimate was done for a band-eliminate filter in [36].

C. THE LOSSY-ACTIVE COUPLING MATRIX

Having a coupling matrix representation of the filter makes the design more versatile. In this section, the new *lossy-active coupling matrix* is introduced as an extension to the lossy coupling matrix. The goal is to integrate the feedback amplifier network as an additional non-resonating node.

The circuit schematic in Fig. 5 (a) depicts the final lossy-active filter when all resonators have the same unloaded quality factor and the resonators 2 through $N-1$ are loss-compensated with the method described in Section II-B.
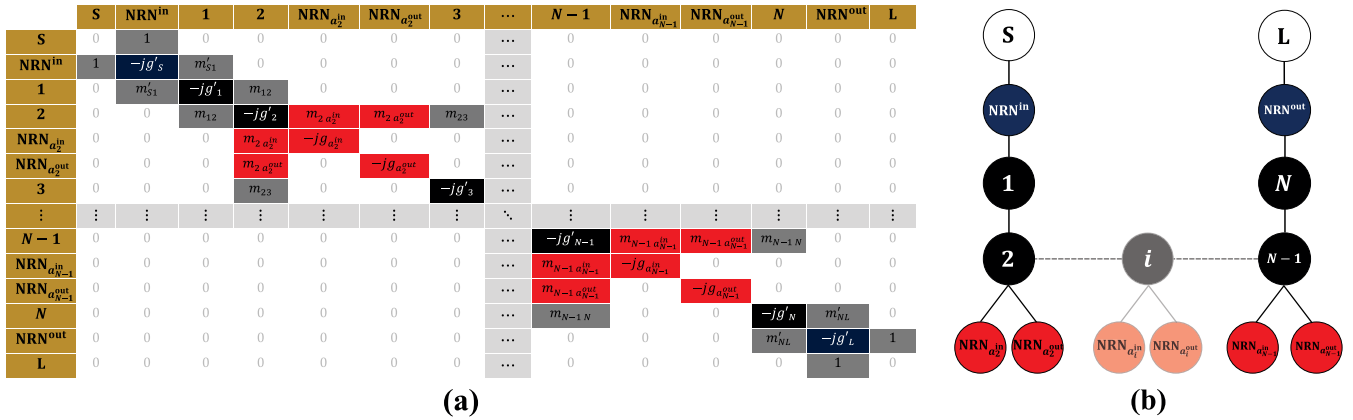
	S	NRN^{in}	1	2	NRN$_{a_2}^{in}$	NRN$_{a_2}^{out}$	3	⋯	N−1	NRN$_{a_{N-1}}^{in}$	NRN$_{a_{N-1}}^{out}$	N	NRN^{out}	L
S	0	1	0	0	0	0	0	⋯	0	0	0	0	0	0
NRN^{in}	1	$-jg'_s$	m'_{S1}	0	0	0	0	⋯	0	0	0	0	0	0
1	0	m'_{S1}	$-jg'_1$	m_{12}	0	0	0	⋯	0	0	0	0	0	0
2	0	0	m_{12}	$-jg'_2$	$m_{2\,a_2^{in}}$	$m_{2\,a_2^{out}}$	m_{23}	⋯	0	0	0	0	0	0
NRN$_{a_2}^{in}$	0	0	0	$m_{2\,a_2^{in}}$	$-jg_{a_2^{in}}$	0	0	⋯	0	0	0	0	0	0
NRN$_{a_2}^{out}$	0	0	0	$m_{2\,a_2^{out}}$	0	$-jg_{a_2^{out}}$	0	⋯	0	0	0	0	0	0
3	0	0	0	m_{23}	0	0	$-jg'_3$	⋯	0	0	0	0	0	0
⋮	⋮	⋮	⋮	⋮	⋮	⋮	⋮	⋱	⋮	⋮	⋮	⋮	⋮	⋮
N−1	0	0	0	0	0	0	0	⋯	$-jg'_{N-1}$	$m_{N-1\,a_{N-1}^{in}}$	$m_{N-1\,a_{N-1}^{out}}$	$m_{N-1\,N}$	0	0
NRN$_{a_{N-1}}^{in}$	0	0	0	0	0	0	0	⋯	$m_{N-1\,a_{N-1}^{in}}$	$-jg_{a_{N-1}^{in}}$	0	0	0	0
NRN$_{a_{N-1}}^{out}$	0	0	0	0	0	0	0	⋯	$m_{N-1\,a_{N-1}^{out}}$	0	$-jg_{a_{N-1}^{out}}$	0	0	0
N	0	0	0	0	0	0	0	⋯	$m_{N-1\,N}$	0	0	$-jg'_N$	m'_{NL}	0
NRN^{out}	0	0	0	0	0	0	0	⋯	0	0	0	m'_{NL}	$-jg'_L$	1
L	0	0	0	0	0	0	0	⋯	0	0	0	0	1	0

(a)

(b)

FIGURE 6. (a): The alternative representation of the lossy-active coupling matrix and (b): the routing diagram for the coupling matrix in (a). This representation includes the input and output nodes of the amplifier as NRN$_{a_i}^{in}$ and NRN$_{a_i}^{out}$, respectively.

The new lossy-active coupling matrix is depicted in Fig. 5 (b) and the routing diagram is given in Fig. 5 (c). The lossy-active coupling matrix has the same entries as the lossy coupling matrix except for the included loss at the resonators 2 through $N-1$ (highlighted in black) and additional active non-resonating nodes that include the amplifier loops as negative resistances. As all the resonators have the same Q_u without the loss compensation, $g'_1 = g'_2 = \ldots = g'_N$ should be satisfied. To be considered a coupling matrix entry, the negative resistances at the non-resonant nodes should be normalized with respect to the center frequency and the bandwidth. This is done by substituting the external quality factor values at the ith active resonator (Q_{1_i} and Q_{2_i}) in (6) for the non-normalized negative resistance in (7) and scaling it so that the ith resonator in Fig. 5 (a) resonates at $\omega_0 = 1/\sqrt{L_i C_i}$ for $i \in \{2, 3, \ldots, N-1\}$. Therefore, each negative normalized conductance (g_{a_i}) in the lossy-active coupling matrix in Fig. 5 (b) is found by:

$$g_{a_i} = \frac{1}{FBW}\left[\frac{1}{Q_{1_i}} - \frac{1}{Q_{2_i}}\left(2G_{Amp_i}\sqrt{\frac{Q_{2_i}}{Q_{1_i}}} - 1\right)\right],$$
$$\text{where } i \in \{2, 3, \ldots, N-1\}. \quad (12)$$

When the external quality factors Q_{1_i} and Q_{2_i} and the amplifier gain in each active resonator G_{Amp_i} satisfy the equality given in (8), it can be shown that the normalized negative conductance g_{a_i} has the exact same magnitude as g'_i in the lossy-active coupling matrix. For the lowest noise figure contribution, they also need to attain the values given in (10).

The value of the additional coupling coefficient, m_{ia_i} in Fig. 5 (b), is also critical for coupling each active non-resonant node to the resonating node of the ith active resonator. It can be found by considering the fact that the coupling matrix entries between the nodes are normalized admittance inverter values. In that regard, for the ith resonant node such that $i \in \{2, 3, \ldots, N-1\}$ to see the exact shunt negative conductance of (12), the value of the coupling coefficient is given as: $m_{ia_i} = \pm g_{a_i}$.

The lossy-active coupling matrix model that is proposed in this section models the input and output coupling of the amplifier as embedded within the active non-resonant node rather than considering them as separate coupling coefficients. An alternative model is given in the next section.

D. ALTERNATIVE REPRESENTATION OF THE LOSSY-ACTIVE COUPLING MATRIX

Rather than considering the loss compensation network as a single node, the input and output nodes of the amplifier can also be considered as separate non-resonant nodes.

Splitting up the input and output nodes of the amplifier network, an alternative representation of the lossy-active coupling matrix is depicted in Fig. 6 with a new routing diagram. The new nodes NRN$_{a_i^{in}}$ and NRN$_{a_i^{out}}$ in the routing diagram represent the input and the output nodes of the ith feedback amplifier, such that $i \in \{2, 3, \ldots, N-1\}$. In this coupling matrix, the shunt conductances at the amplifier input and output are denoted as $g_{a_i^{in}}$ and $g_{a_i^{out}}$, respectively. Their values are found by separating the negative normalized conductance in (12) as:

$$g_{a_i^{in}} = \frac{1}{FBW \cdot Q_{1_i}},$$
$$g_{a_i^{out}} = -\frac{1}{FBW \cdot Q_{2_i}}\left(2G_{Amp_i}\sqrt{\frac{Q_{2_i}}{Q_{1_i}}} - 1\right),$$
$$\text{where } i \in \{2, 3, \ldots, N-1\}. \quad (13)$$

The coupling coefficient between the amplifier input and its corresponding resonator is given by: $m_{ia_i^{in}} = \pm g_{a_i^{in}}$, whereas the coupling between amplifier output and the resonator is given by: $m_{ia_i^{out}} = \pm g_{a_i^{out}}$. It should be noted that the coupling configuration in Fig. 6 does not take into account the coupling between the amplifier input and output, however, the effect of the input signal on the output is already embedded in (13).
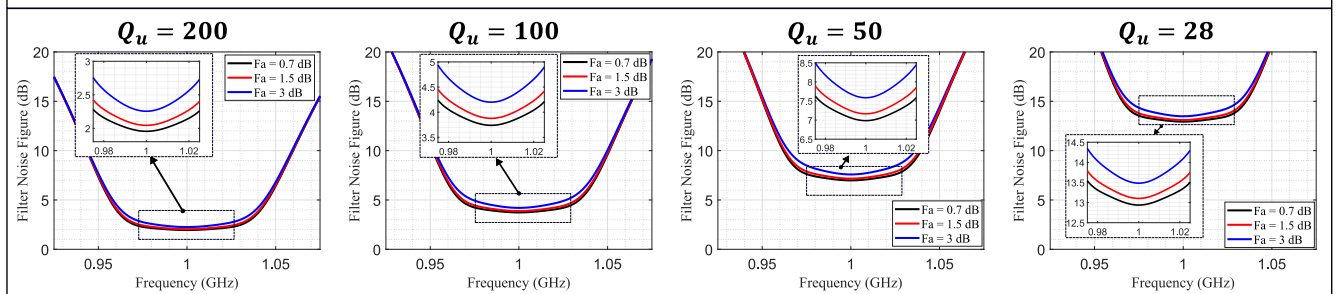
III. DESIGN AND ANALYSIS

To verify the proposed approach and demonstrate designs of different order, this section evaluates the performance of the
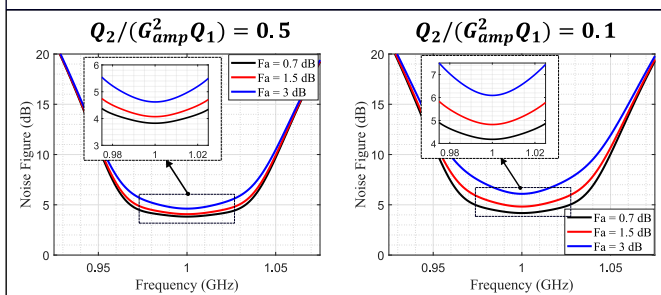
(a) Filter Response
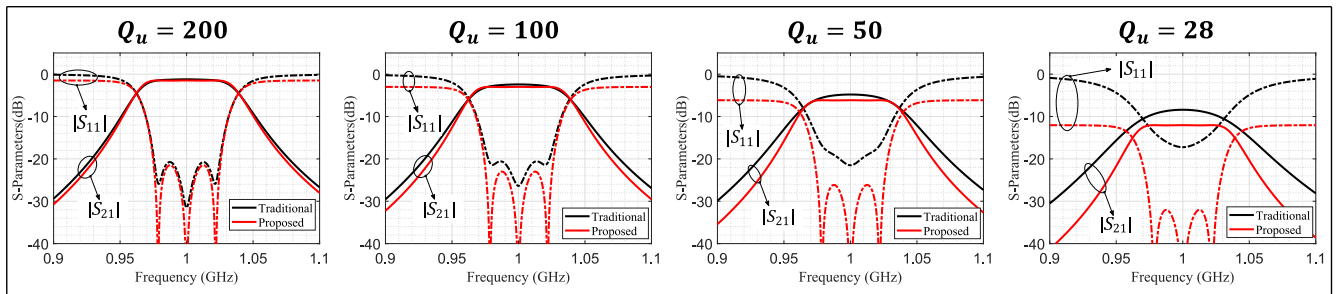
(b) Noise Figure, $Q_2/(G_{amp}^2 Q_1) = 1$

(c) Noise Figure, $Q_u = 100$

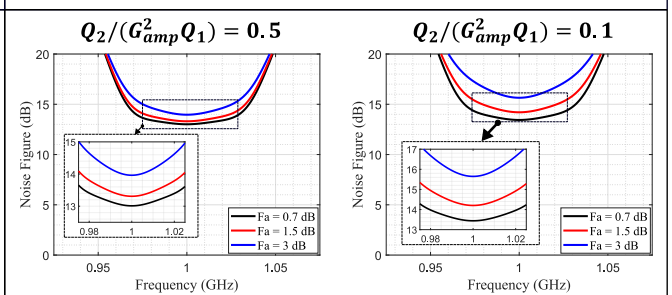## (d) Noise Figure, $Q_u = 28$

FIGURE 7. (a): Recovery of the filter responses with the use of the proposed approach. Four different filter examples with quality factors of 200, 100, 50, and 28 in each resonator are depicted. For comparison, the responses of traditional design with the same quality factors on each resonator are also shown. The solid lines demonstrate $|S_{11}|$ and the dashed lines illustrate $|S_{21}|$ of each filter. (b): Theoretical noise figure responses of the proposed designs in (a). The figure shows the noise figures for an amplifier with different noise figure values. (c) and (d): Noise figure responses when the amplifier input and output coupling inverters are not properly tuned.

method for different loss levels. For that purpose, filters of third-, fourth-, and fifth-order are designed using the circuit topology given in Fig. 5 (a).

The third-order filter examples include designs with resonator quality factor values of 200, 100, 50, and 28 which correspond to insertion loss values of 1.49 dB, 3 dB, 6.17 dB, and 12 dB, respectively. The fourth- and fifth-order design examples include filters with insertion loss values of 3 dB and 12 dB. To have these insertion loss values, the corresponding quality factors are calculated as 108 and 31 for the fourth-order and 114 and 32 for the fifth-order filters. The designs are performed by denormalizing the lossy-active coupling matrix for a center frequency of 1 GHz and 5 % FBW.

The transmission and reflection responses of the filters are depicted in Fig. 7 (a) for the third-order case and in Fig. 8 (a) and (b) for the fourth- and fifth-order designs, respectively. The same figures also show the responses of the

conventionally designed (i.e., using the g-coefficients) filters when each of their resonators has quality factors of 200, 100, 50, and 28 for the third-order, 108 and 31 for the fourth-order, and 114 and 32 for the fifth-order. Other parameters of the eight different designs, including the attenuation factor (k), noise figure, and insertion loss are listed in Table 1.

As observed in Fig. 7 (a), the third-order filters designed with the proposed approach have the prescribed equiripple responses with the desired FBW and center frequencies. Not only can the proposed design reconstruct the response of the filter having a Q_u of 200 for each resonator, but it can also accomplish that for the severely perturbed transmission and reflection responses of the filter having a Q_u of 28 in each resonator. Further observing Fig. 7 (a), it should also be noted that the shape recovery is achieved at the cost of additional IL for the third-order designs. This additional loss will be referred to as the accepted loss (AL) and is defined as the
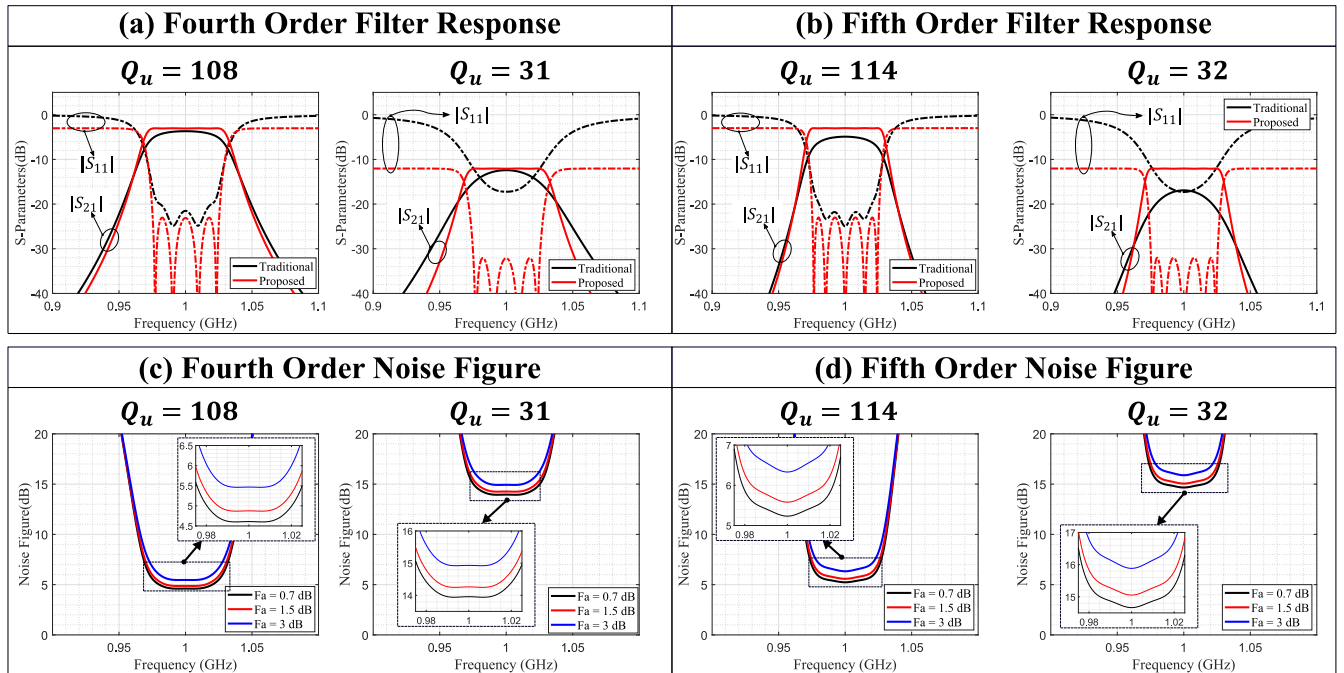
FIGURE 8. Filter responses of the fourth- and fifth-order design examples are depicted in (a) and (b) whereas their noise figure responses are depicted in (c) and (d), respectively. As in Fig. 7, the filter responses are compared with the corresponding design examples which have resonators of the same quality factors as in their lossy counterpart.

TABLE 1. Parameters of the design examples of order three, four, and five. In the table, *k* denotes the attenuation factor, IL denotes the insertion loss, AL stands for the accepted loss, RcL is for recovered loss, and NF depicts the noise figure of the filters when amplifier external quality factors satisfy (9).

	Ord.	k	IL (dB)	Q_u	AL/RcL (dB)	NF (dB)
Ex.1	3	0.918	1.49	200	0.26 (A)	1.94
Ex.2 (FML)	3	0.841	3	100	0.57 (A)	3.75
Ex.3	3	0.701	6.17	50	1.33 (A)	7.16
Ex.4 (FHL)	3	0.500	12	28	3.63 (A)	12.94
Ex.5	4	0.841	3	108	0.38 (Rc)	4.60
Ex.6	4	0.5	12	31	0.26 (Rc)	13.95
Ex.7	5	0.841	3	114	1.93 (Rc)	5.23
Ex.8	5	0.5	12	32	4.92 (Rc)	14.66

difference between the insertion loss of the traditional and the proposed designs. Comparing the responses in Fig. 7 (a), it is observed that both the insertion loss and the accepted loss levels increase with the reduced resonator quality factors.

The fourth- and fifth-order filter responses, which are designed to have insertion loss values of 3 dB and 12 dB, are shown in Fig. 8 (a) and (b). As observed, these designs also have the prescribed filter responses. The shape perturbation in the conventional designs gets more severe as the filter order increases, which emphasizes the importance of the proposed method. While resonator quality factors at the order of 100 can produce acceptable filter responses using the traditional design of third-order, the same resonators yield significant filter shape degradation and additional insertion loss for the fourth- and fifth-order designs.

Unlike the third-order case, for the response of fourth- and fifth-order designs, the insertion loss of the proposed approach is *lower* than that of the conventional method. This is due to the fact that the number of loss-compensated resonators increases in the higher-order filters. In that case, the difference between the insertion loss of the traditional and the proposed approach is referred to as the *recovered loss* (RcL) in Table 1.

To examine the noise figure of the designs and the effect of the feedback amplifier noise figure on it, Fig. 7 (b) depicts the simulated filter noise figures for three different amplifiers. These simulations are performed in AWR (Cadence Design Systems, San Jose, CA) design environment. The simulation models contain closed-form lumped and distributed elements. Furthermore, the compensation network uses the non-linear amplifier model with a flat gain of 15 dB within the frequency band of 0.5 GHz to 1.5 GHz. The input and output of the amplifier are matched to 50 Ω and the specified noise figure values in Fig. 7 (b) are for a 50 Ω source.

For the amplifier noise figure values of 0.7 dB, 1.5 dB, and 3 dB, the simulated noise figures of the third-order designs are depicted in Fig 7 (b) when the external quality factors due to the amplifier (Q_1 and Q_2) satisfy the minimum noise condition in (9) and (10). As observed, an increase of 2.3 dB in the amplifier noise figure yields a filter noise figure increase of 0.54 dB and 0.46 dB when filter resonator quality factors are 28 and 100, respectively. Considering these results, it is seen that the increased amplifier noise figure has a minor impact on the overall noise figure of the third-order designs, as long as (9) is satisfied.

$$
M_{FML}=
\begin{array}{c|cccccccc}
 & S & NRN & 1 & 2 & NRN & 3 & NRN & L \\
\hline
S & 0 & 1 & 0 & 0 & 0 & 0 & 0 & 0 \\
NRN & 1 & -0.171j & 1.067 & 0 & 0 & 0 & 0 & 0 \\
1 & 0 & 1.067 & -0.200j & 1.030 & 0 & 0 & 0 & 0 \\
2 & 0 & 0 & 1.030 & -0.200j & 0.200 & 1.030 & 0 & 0 \\
NRN & 0 & 0 & 0 & 0.200 & 0.200j & 0 & 0 & 0 \\
3 & 0 & 0 & 0 & 1.030 & 0 & -0.200j & 1.067 & 0 \\
NRN & 0 & 0 & 0 & 0 & 0 & 1.067 & -0.171j & 1 \\
L & 0 & 0 & 0 & 0 & 0 & 0 & 1 & 0 \\
\end{array}
$$

$$
M_{FHL}=
\begin{array}{c|cccccccc}
 & S & NRN & 1 & 2 & NRN & 3 & NRN & L \\
\hline
S & 0 & 1 & 0 & 0 & 0 & 0 & 0 & 0 \\
NRN & 1 & -0.600j & 0.866 & 0 & 0 & 0 & 0 & 0 \\
1 & 0 & 0.866 & -0.703j & 1.030 & 0 & 0 & 0 & 0 \\
2 & 0 & 0 & 1.030 & -0.703j & 0.703 & 1.030 & 0 & 0 \\
NRN & 0 & 0 & 0 & 0.703 & 0.703j & 0 & 0 & 0 \\
3 & 0 & 0 & 0 & 1.030 & 0 & -0.703j & 0.866 & 0 \\
NRN & 0 & 0 & 0 & 0 & 0 & 0.866 & -0.600j & 1 \\
L & 0 & 0 & 0 & 0 & 0 & 0 & 1 & 0 \\
\end{array}
$$

FIGURE 9. The lossy-active coupling matrices of the FML and the FHL. The matrices are denoted as M_{FML} and M_{FHL}, respectively. In the illustrations, the feedback amplifier network is considered as a negative resistance, as presented in Section II-C.

Another important point is that the external quality factors Q_1 and Q_2 greatly affect the overall filter noise figure. It was shown in [35]–[37] that slight external coupling variations that violate (9) yield significant filter noise figure degradations. To illustrate that, the third order designs with resonator Q_u values of 100 and 28 are simulated with detuned amplifier input and output coupling as given in Fig. 7 (c) and (d). The corresponding S_{11} and S_{21} responses of the filters in Fig. 7 (c) and (d) match the ones in Fig. 7 (a) as Q_1 and Q_2 still satisfy the loss compensation condition given by (8). The effect of the increasing amplifier noise figure is exacerbated by the detuned coupling mechanisms. In particular, the 2.3 dB of amplifier noise figure increase yields a noise figure increase of 0.79 dB when $Q_2/G_{amp}^2\,Q_1 = 0.5$ and 1.9 dB when that ratio is 0.1 for the case of $Q_u = 100$. Therefore, this noise figure sensitivity should also be taken into account if the minimum noise figure is desired.

Finally, the noise figure responses of the fourth- and fifth-order designs are depicted in Fig. 8 (c) and (d), respectively. It should be noted that the amplifiers at the active networks in each design are identical and have a gain of 15 dB as in the third-order case. The noise figures of the active filters increase further beyond their corresponding insertion losses, as the order of the filter increases. Furthermore, the sensitivity of the filter noise figure also increases when the noise figure of the amplifiers gets higher in the higher-order designs.

IV. METHODS OF IMPLEMENTATION

Among the examples in the previous section, the third-order filters with resonator quality factors of 100 and 28 are implemented using microstrip technology. These prototypes are referred to as the filter with moderate loss (FML) and the filter with high loss (FHL), respectively. Their corresponding lossy-active coupling matrices are depicted in Fig. 9. As observed, the lossy-active coupling matrices have negative imaginary entries at the diagonal elements, which represent the loss at each resonating and non-resonant node. Furthermore, each matrix also includes a diagonal entry with a positive imaginary term, representing the negative conductance at each active node. The magnitude of the normalized resistance at the second resonating node is equal to the magnitude of

the active negative resistance, which corresponds to full loss compensation in the middle resonator of the lossy-active filter prototypes.

Using the lossy-active coupling matrices, the initial step in filter implementation is design of the lossy resonators, according to their lumped equivalents in Fig. 5 (a). Considering that half-wave open-ended microstrip lines emulate parallel RLC resonators, the equivalent lumped impedance parameters are given as in the following [38]:

$$
R_m = \frac{Z_0}{\alpha l}, \quad C_m = \frac{\pi}{2\omega_0 Z_0}, \quad L_m = \frac{1}{w_0^2 C}, \tag{14}
$$

where R_m, L_m, and C_m denote the equivalent resistance, inductance, and the capacitance of the microstrip resonator and α is the attenuation constant (Nepers/m). Using (14), the quality factor can be calculated as $Q_{u_m} = R_m/\omega_0\,L_m$.

While the quality factor of 100 can be achieved with a microstrip resonator alone, the required Z_0 to get a Q_u of 28 is impractically high. Therefore, shunt resistors are used at both ends of the half-wave microstrip lines to reduce the Q_u of the resonators down to 28 for the FHL.

The inter-resonator coupling mechanisms are implemented using parallel edge-coupling and the desired coupling strength (M_{ij}) is achieved using:

$$
M_{ij} = FBW \cdot m_{ij}, \tag{15}
$$

where m_{ij} is the coupling coefficient between i^{th} and j^{th} resonator in the coupling matrix given by Fig. 5 (b).

The input and output admittance inverters are realized using quarter-wave transformers in both designs. Their characteristic impedances are calculated by denormalizing the coupling matrix entries (m'_{S1}) and (m'_{3L}). The unit impedance inverters connected to the first and last resonators in the coupling matrix of Fig. 5 (b) are scaled to have quarter-wave lines with realizable characteristic impedance values.

To implement the amplifier coupling at the middle resonator, edge coupling is used. The external quality factors Q_1 and Q_2 are calculated using (10). The amplifier for achieving an infinite Q_u at the middle resonator is chosen to have a flat gain of 15 dB at the 0.8 to 1.2 GHz band.

The circuit-based simulations of the designs are carried out in AWR, whereas the electromagnetic (EM) simulations
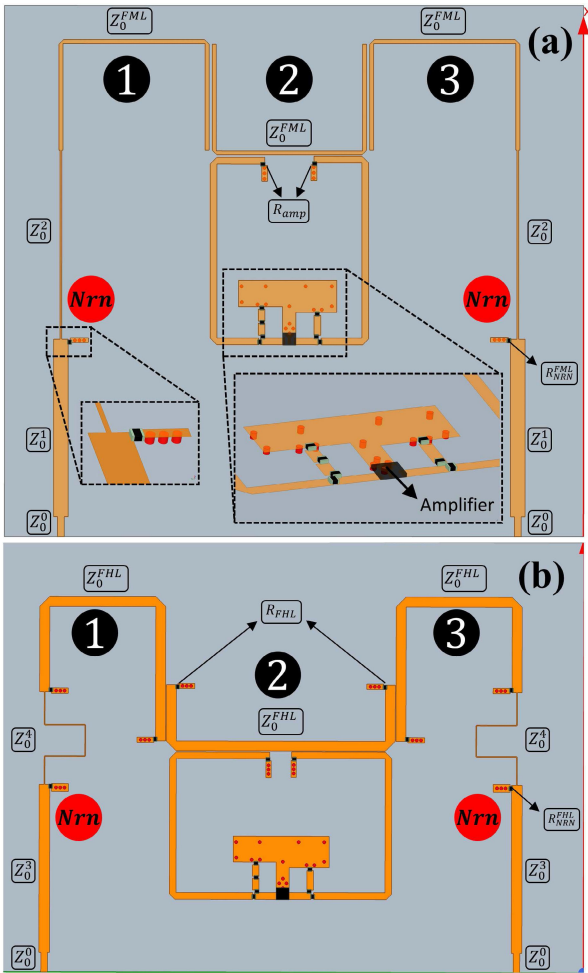
FIGURE 10. The HFSS layouts of the filters. (a): Layout of the FML with magnified 3-D views at the non-resonant node and the amplifier network. (b): Layout of the FHL. The characteristic impedances, resonating and non-resonant nodes, and the resistors of both prototypes are marked and their values are shown in Table 2.

TABLE 2. The characteristic impedance and resistance values of the FML and FHL, as depicted in Fig. 10.

Characteristic Impedances (Ω)						
Z_0^0	Z_0^1	Z_0^2	Z_0^3	Z_0^4	Z_0^{FML}	Z_0^{FHL}
50	29.9	98.6	36.8	125.4	67.6	38.4

Resistances (Ω)			
R_{amp}	R_{FHL}	R_{NRN}^{FML}	R_{NRN}^{FHL}
50	1500	82	45

30-mil-thick substrate with a copper thickness of 17.5 μm. For precise board patterning, an LPKF ProtoLaser U4 (LPKF, Garbsen, Germany) was used. For the lumped capacitors at the amplifier network, multilayer ceramic capacitors from Murata Electronics (Kyoto, Japan) and for the RF-choke inductors, Murata spiral inductors were used. For the amplifiers of the loss compensation networks, PGA-103 low noise amplifier from Mini-Circuits (Brooklyn, NY) was used with its prescribed stabilization network [39].
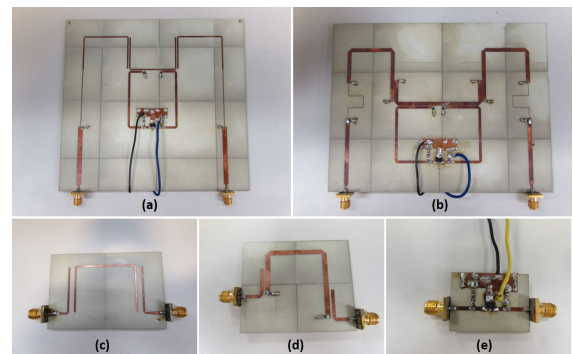

FIGURE 11. The fabricated prototypes. (a): FML, (b): FHL, (c): A single resonator of FML, (d): A single resonator of FHL, and (e): The feedback amplifier in the loss compensation network.

The fabricated prototypes of the FML and the FHL are depicted in Fig. 11 (a) and (b), respectively. To account for the discrepancies between simulated and actual resonator properties, a single resonator of each design was fabricated and measured. In order to measure the resonant frequencies and quality factors of the resonators, they are weakly coupled to the input and output ports using edge coupling, as depicted in Fig. 11 (c) and (d). The measured quality factors of the single resonators at 1 GHz are 132.2 and 24.6 for the FML and FHL, respectively. After tuning for the slightly higher measured Q_u, it was observed in the simulations that the FML yields a response with approximately 4% of FBW at an insertion loss level of 3 dB. For the case of FHL, the measured quality factor was close enough to the simulated one, so it did not noticeably change the response.

To precisely determine the forward gain, phase contribution, noise figure, and the non-linearity of the amplifier, a single amplifier network is also fabricated and measured,

are done in HFSS Electromagnetic Suite (ANSYS, Cannonsburg, PA). The HFSS layouts of the prototypes are depicted in Fig. 10. In that figure, transmission line impedances within the filter network are marked with the superscripts of Z_0. The characteristic impedances of the FML and FHL resonators are denoted as Z_0^{FML} and Z_0^{FHL}. Similarly, the termination resistors of the amplifier are denoted with R_{amp}, shunt resistors at non-resonating nodes of FML and FHL are shown as R_{NRN}^{FML} and R_{NRN}^{FHL}, and the shunt resistors to adjust the quality factors of FHL resonators are called as R_{FHL}, respectively. The values of these parameters after tuning are shown in Table 2.

The physical dimensions of the FML and FHL are given as (14.6 cm × 13.9 cm) and (14.6 cm × 11.3 cm), respectively. It should be noted that no attempts were made to miniaturize the prototypes as the goal of this study was to demonstrate the shape correction.

V. FABRICATION AND MEASUREMENTS
To validate the proposed method, both prototypes were fabricated on a RO 4350B LoPro (Rogers Corp., Chandler, AZ)

as depicted in Fig. 11 (e). The gain of the amplifier is measured to be approximately 15.6 dB and the noise figure is around 0.69 dB at a frequency of 1 GHz. To get accurate phase response measurements, the SMA connector lengths were de-embedded from the measured amplifier parameters in simulations. The 1-dB input and output compression points (IP1dB and OP1dB) of the amplifier are measured as 7.9 dBm and 22.5 dBm whereas the input and output third-order intercept points (IIP3 and OIP3) are measured as 26.5 dBm and 41.9 dBm. Furthermore, the DC power consumption of the prototypes are measured as 0.5 W. For an Nth order active filter using the proposed design technique, therefore, the power consumption is approximated as $(N - 2) \times P_{Amp}$, where P_{Amp} is the power consumption of the feedback amplifier within its linear operating region.

S_{11} and S_{21} measurements of the both prototypes are performed using an Agilent PNA N5225A (Keysight Technologies, Santa Rosa, CA) network analyzer. The noise figure measurements were taken with an Agilent PSA E4448A spectrum analyzer and an Agilent 346B calibrated noise source. For the noise figure measurements, the Y-Factor method [40] was used with a measurement bandwidth of 1 MHz and 10 averages. Furthermore, an external LNA was cascaded to the network and the noise figure of a 15 dB attenuator is measured with the same setup to verify the accuracy of the measurements. IP1dB and OP1dB of the prototypes at 1 GHz are measured using an Agilent signal generator, the Agilent PSA E4448A spectrum analyzer, and a highly linear Mini-Circuits power amplifier (ZHL-10W-2G+) with 43.4 dB gain, 41.72 dBm OP1dB, and 53.5 dBm OIP3. The IIP3 and OIP3 levels of the prototypes are measured using the same signal source, power amplifier, and spectrum analyzer with 1 MHz tone spacing.

The theoretical and measured S-parameters for the FML and FHL are depicted in Figure 12. As observed, there is good agreement between the measured and theoretical responses for the FML. The measured insertion loss of FML is 2.92 dB at 1 GHz and its FBW is 4.2 %. The slightly narrower bandwidth is a result of re-tuning the design in order to account for the slightly higher measured quality factors than expected. For FHL, the measured and theoretical transmission responses are in good agreement with the fabricated prototype having an insertion loss of 11.82 dB. Considering the reflection response, the three pole locations are at the correct frequencies, however, the slightly detuned input and output coupling inverters cause a slight mismatch between the measured and theoretical responses. Overall, both prototypes have the desired filter response and selectivity.

The theoretical and measured noise figures of the FML and the FHL are also depicted in Fig. 11. The measured noise figure values of the designs are 5.19 dB for FML and 14.2 dB for FHL at 1 GHz, whereas the theoretical values are 3.76 dB and 12.97 dB, respectively. It should be noted that the theoretical noise figure results come from the AWR simulations with closed-form lumped elements and do not take into account the losses due to the microstrip line inverters. The reason
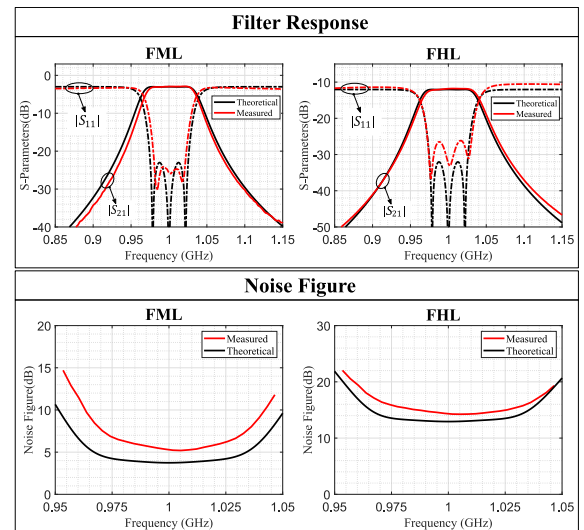

FIGURE 12. Comparison of the theoretical and measured responses. The first row depicts the filter responses of FML and FHL whereas the second row demonstrates the noise figure responses. For the filter responses, the solid lines depict the $|S_{11}|$ and the dashed lines illustrate the $|S_{21}|$ of each filter.

for including those simulation results was to demonstrate the theoretically achievable noise figure for both prototypes. Another reason for the discrepancies between the simulated and measured noise figures is the re-tuned input and output coupling inverters of the amplifier to achieve the best shape correction.

Finally, the non-linearity performances of the prototypes are depicted in the table of Fig. 13. As both prototypes attenuate the input signal, the input-related non-linearity metrics (IP1dB and IIP3) and the output-related measurements (OP1dB and OIP3) are considered separately. As observed, the input compression point of FML is much higher than that of the FHL for a simple reason that the insertion loss difference between the amplifier ON and OFF states is much higher in FHL. In other words, a higher percentage of the energy is passing through the amplifier in FHL to compensate for the lower quality factor. An important point to be observed is that the input compression point and the third intercept of both prototypes are better than that of the amplifier that is used within the design of the prototypes. This is a result of the input power to the filter being shared within the resonators and the active network. This way, the amplifier is exposed to less power than the incoming input power to the active filter.

The table in Fig. 13 provides a comparison of several performance metrics of the related studies in the literature. The compared studies include the applications of active filters and lossy filters separately. To that end, the proposed method in this study is a hybrid implementation of lossy filters and active filters. Results of the two example prototypes show that the proposed design approach is realizable and the shape correction can be achieved using resonators with arbitrary quality factors. It should be noted that the shape correction is achieved at the cost of increased noise figure and

Ref	Resonator Type	Techniques	Order	f_0 (GHz)/ FBW	Q_u	IL/IG (dB)	TZ	NF (dB)	IP1dB (dBm)	OP1dB (dBm)	IIP3 (dBm)	OIP3 (dBm)
[21]	Microstrip	Lossy, Non-Unif. Q	6	0.96/6.2%	250-80	7.2	Yes	*	**	**	**	**
[30]	Microstrip	Lossy, Equalized Q	4	1/11.5%	200	3	Yes	*	**	**	**	**
[28]	Microstrip	Lossy, Non-Unif. Q	6	3.8/21%	95-57-35	2.5	Yes	*	**	**	**	**
[29]	double-layered coupled resn.	Lossy, Equalized Q	6	0.97/25.7%	120	3.4	Yes	*	**	**	**	**
[32]	Microstrip	Lossy, Equalized Q	4	0.925/9.2%	230	≈8.5	No	*	**	**	**	**
[26]	Combline Cavity	Lossy, Equalized Q	4	11.18/1%	1300	≈2.9	No	*	**	**	**	**
[4]	MMIC, λ/4 line	HEMT-Negative Resistance	2	60	***	2.8	Yes (I/O Coupl.)	10.5	8.8	5	***	***
[17]	MMIC, Lumped	Resonator Link with FET	3	1.9	***	12 (IG)	No	6.2	***	***	***	***
[14]	PCB Lumped Active Inductor	Class-AB BJT Active Inductor	2	0.7/5% (3-dB FBW)	***	7.2	No	10	***	12	***	***
[8]	Microstrip	Parametric Active	3	2.03/8%	***	0.22	No	3.7	***	17	***	26.5
[34]	SIW	Filtering Amplifier	2	10/5%	***	9 (IG)	No	≈3	≈ −5.5	≈ 5.5	***	***
FML	Microstrip	Hybrid	3	1/5%	131.2	2.89	No	5.19	38.1	34.1	46.94	44.05
FHL	Microstrip	Hybrid	3	1/5%	24.6	11.9	No	14.2	26.4	13.4	46	34.1

*   Noise figure of passive filters will be equivalent to the reciprocal of their available power gain, or to their attenuation if perfectly matched at input and output.
**   Passive filters are assumed to be linear and the information of P1dB and IP3 are not reported.
*** The data is not explicitly reported in the corresponding study.
IG: Insertion gain, TZ: Transmission zero.

Lossy Microwave Filters
Active Filters
Proposed Hybrid Lossy-Active Technique

FIGURE 13. Table of comparison with other relevant studies in literature.

non-linearity when the resonator quality factors are very low. Therefore, the initial consideration with this design approach is to use resonators with the highest achievable quality factors within the design limits. Depending on the design, a pre-amplifier stage might be required to compensate for both the noise figure and the insertion loss if the available resonators have very low quality factors. This results in the prescribed filter selectivity with no insertion loss and reduced noise figure, which cannot be achieved by amplifying a perturbed filter response.

VI. CONCLUSION AND DISCUSSION

Using the coupling matrix theory for highly lossy applications has always been a challenge for filter designers due to severe response shape degradations. In this study, a new method of synthesizing lossy filters with the use of an active quality factor enhancement method is presented. Unlike most active filter approaches, in which the active quality factor enhancement is used in every resonator, this study aims to minimize the number of active elements within the design.

For the design stage, a new concept of *lossy-active coupling matrix* is introduced. With that approach, this study represents an initial transfer of the lossy filter design theory to the highly lossy applications such as PCB-based or MMIC filters. Using the lossy-active coupling matrix and possible matrix rotations, higher-order filters can be designed using resonators with arbitrary quality factors. This will require future solutions including active inter-resonator coupling mechanisms. Therefore, the design theory in this study provides a new step towards implementing high selectivity filters with prescribed responses using resonators with limited quality factors. This proposed method facilitates the future integration of analog filters with improved performance into receiver front ends in system-on-a-chip applications.

REFERENCES

[1] R. J. Cameron, "General coupling matrix synthesis methods for chebyshev filtering functions," *IEEE Trans. Microw. Theory Techn.*, vol. 47, no. 4, pp. 433–442, Apr. 1999.

[2] R. Cameron, "Advanced coupling matrix synthesis techniques for microwave filter," *IEEE Trans. Microw. Theory Techn.*, vol. 51, no. 1, pp. 1–10, Jan. 2003.

[3] C.-Y. Chang and T. Itoh, "Microwave active filters based on coupled negative resistance method," *IEEE Trans. Microw. Theory Techn.*, vol. 38, no. 12, pp. 1879–1884, Dec. 1990.

[4] M. Ito, K. Maruhashi, S. Kishimoto, and K. Ohata, "60-GHz-band coplanar MMIC active filters," *IEEE Trans. Microw. Theory Techn.*, vol. 52, no. 3, pp. 743–750, Mar. 2004.

[5] S. Saeedi, S. Atash-Bahar, and H. H. Sigmarsson, "Active tunable substrate integrated evanescent-mode cavity resonator using negative resistance," in *Proc. IEEE Radio Wireless Symp. (RWS)*, Jan. 2016, pp. 87–90.

[6] R. Kaunisto, K. Stadius, and V. Porra, "Active mmic filters with negative resistance compensation," *Electron. Lett.*, vol. 34, no. 12, pp. 1236–1237, 1998.

[7] L. K. Yeung, X. Zou, and Y. E. Wang, "Parametric quality factor enhancement for highly-selective miniaturized BPFs," in *Proc. IEEE Radio Wireless Symp. (RWS)*, Jan. 2020, pp. 148–151.

[8] L. K. Yeung, X. Zou, and Y. E. Wang, "BPFs with parametrically compensated passband insertion loss and selectivity," in *IEEE MTT-S Int. Microw. Symp. Dig.*, Aug. 2020, pp. 803–806.

[9] S. Lucyszyn and I. D. Robertson, "Monolithic narrow-band filter using ultrahigh-Q tunable active inductors," *IEEE Trans. Microw. Theory Techn.*, vol. 42, no. 12, pp. 2617–2622, Dec. 1994.

[10] Y. Wu, X. Ding, M. Ismail, and H. Olsson, "RF bandpass filter design based on CMOS active inductors," *IEEE Trans. Circuits Syst. II, Analog Digit. Signal Process.*, vol. 50, no. 12, pp. 942–949, Dec. 2003.

[11] R. V. Snyder and D. L. Bozarth, "Analysis and design of a microwave transistor active filter," *IEEE Trans. Microw. Theory Techn.*, vol. MTT-18, no. 1, pp. 2–9, Jan. 1970.

[12] D. K. Adams and R. Y. C. Ho, "Active filters for UHF and microwave frequencies," *IEEE Trans. Microw. Theory Techn.*, vol. MTT-17, no. 9, pp. 662–670, Sep. 1969.

[13] G. Leuzzi, V. Stornelli, L. Pantoli, and S. Del Re, "Single transistor high linearity and wide dynamic range active inductor," *Int. J. Circuit Theory Appl.*, vol. 43, no. 3, pp. 277–285, Mar. 2015. [Online]. Available: https://onlinelibrary.wiley.com/doi/abs/10.1002/cta.1938

[14] L. Pantoli, V. Stornelli, and G. Leuzzi, "High dynamic range, low power, tunable, active filter for RF and microwave wireless applications," *IET Microw., Antennas Propag.*, vol. 12, no. 4, pp. 595–601, Mar. 2018. [Online]. Available: https://ietresearch.onlinelibrary.wiley.com/doi/abs/10.1049/iet-map.2017.0685

[15] W. Schwab and W. Menzel, "A low-noise active bandpass filter," *IEEE Microw. Guided Wave Lett.*, vol. 3, no. 1, pp. 1–2, Jan. 1993.

[16] Y.-H. Chun, S.-W. Yun, and J.-K. Rhee, "Active impedance inverter: Analysis and its application to the bandpass filter design," in *IEEE MTT-S Int. Microw. Symp. Dig.*, vol. 3, Jun. 2002, pp. 1911–1914.

[17] S. F. Sabouri, "A GaAs MMIC active filter with low noise and high gain," in *IEEE MTT-S Int. Microw. Symp. Dig.*, vol. 3, Jun. 1998, pp. 1177–1180.

[18] W. Jutzi, "Microwave bandwidth active transversal filter concept with MESFETs," *IEEE Trans. Microw. Theory Techn.*, vol. MTT-19, no. 9, pp. 760–767, Sep. 1971.

[19] M. J. Schindler and Y. Tajima, "A novel MMIC active filter with lumped and transversal elements," in *Dig. Papers., Microw. Millimeter-Wave Monolithic Circuits Symp.*, 1989, pp. 57–60.

[20] M. Dishal, "Design of dissipative band-pass filters producing desired exact amplitude-frequency characteristics," *Proc. IRE*, vol. 37, no. 9, pp. 1050–1069, Sep. 1949.

[21] A. C. Guyette, I. C. Hunter, and R. D. Pollard, "The design of microwave bandpass filters using resonators with nonuniform Q," *IEEE Trans. Microw. Theory Techn.*, vol. 54, no. 11, pp. 3914–3922, Nov. 2006.

[22] A. C. Guyette, I. C. Hunter, and R. D. Pollard, "A new class of selective filters using low-Q components suitable for MMIC implementation," in *IEEE MTT-S Int. Microw. Symp. Dig.*, vol. 3, Jun. 2004, pp. 1959–1962.

[23] A. C. Guyette, I. C. Hunter, and R. D. Pollard, "Exact synthesis of microwave filters with nonuniform dissipation," in *IEEE MTT-S Int. Microw. Symp. Dig.*, Jun. 2007, pp. 537–540.

[24] M. Meng and I. C. Hunter, "The design of parallel connected filter networks with non-uniform q resonators," in *IEEE MTT-S Int. Microw. Symp. Dig.*, Jun. 2012, pp. 1–3.

[25] M. Yu and V. Miraftab, "Shrinking microwave filters," *IEEE Microw. Mag.*, vol. 9, no. 5, pp. 40–54, Oct. 2008.

[26] V. Miraftab and M. Yu, "Generalized lossy microwave filter coupling matrix synthesis and design using mixed technologies," *IEEE Trans. Microw. Theory Techn.*, vol. 56, no. 12, pp. 3016–3027, Dec. 2008.

[27] V. Miraftab and M. Yu, "Advanced coupling matrix and admittance function synthesis techniques for dissipative microwave filters," *IEEE Trans. Microw. Theory Techn.*, vol. 57, no. 10, pp. 2429–2438, Oct. 2009.

[28] A. Basti, A. Périgaud, S. Bila, S. Verdeyme, L. Estagerie, and H. Leblond, "Design of microstrip lossy filters for receivers in satellite transponders," *IEEE Trans. Microw. Theory Techn.*, vol. 62, no. 9, pp. 2014–2024, Sep. 2014.

[29] J. Ni, J. Hong, and P. M. Iglesias, "Compact microstrip IF lossy filter with ultra-wide stopband," *IEEE Trans. Microw. Theory Techn.*, vol. 66, no. 10, pp. 4520–4527, Oct. 2018.

[30] J. Mateu, A. Padilla, C. Collado, M. Martinez-Mendoza, E. Rocas, C. Ernst, and J. M. O'Callaghan, "Synthesis of 4th order lossy filters with uniform q distribution," in *IEEE MTT-S Int. Microw. Symp. Dig.*, May 2010, pp. 568–571.

[31] L. Szydlowski, A. Lamecki, and M. Mrozowski, "Design of microwave lossy filter based on substrate integrated waveguide (SIW)," *IEEE Microw. Wireless Compon. Lett.*, vol. 21, no. 5, pp. 249–251, May 2011.

[32] R. Das, Q. Zhang, A. Kandwal, and H. Liu, "All passive realization of lossy coupling matrices using resistive decomposition technique," *IEEE Access*, vol. 7, pp. 5095–5105, 2019.

[33] Y. Gao, J. Powell, X. Shang, and M. J. Lancaster, "Coupling matrix-based design of waveguide filter amplifiers," *IEEE Trans. Microw. Theory Techn.*, vol. 66, no. 12, pp. 5300–5309, Dec. 2018.

[34] Y. Gao, F. Zhang, X. Lv, C. Guo, X. Shang, L. Li, J. Liu, Y. Liu, Y. Wang, and M. J. Lancaster, "Substrate integrated waveguide filter–amplifier design using active coupling matrix technique," *IEEE Trans. Microw. Theory Techn.*, vol. 68, no. 5, pp. 1706–1716, May 2020.

[35] M. Nick and A. Mortazawi, "Low phase-noise planar oscillators based on low-noise active resonators," *IEEE Trans. Microw. Theory Techn.*, vol. 58, no. 5, pp. 1133–1139, May 2010.

[36] Y. Ishikawa, S. Yamashita, and S. Hidaka, "Noise design of active feedback resonator BEF," *IEEE Trans. Microw. Theory Techn.*, vol. 41, no. 12, pp. 2133–2138, Dec. 1993.

[37] H. Ezzedine, L. Billonnet, B. Jarry, and P. Guillon, "Optimization of noise performance for various topologies of planar microwave active filters using noise wave techniques," *IEEE Trans. Microw. Theory Techn.*, vol. 46, no. 12, pp. 2484–2492, Dec. 1998.

[38] D. Pozar, *Microwave Engineering*. Hoboken, NJ, USA: Wiley, 2011. [Online]. Available: https://books.google.com/books?id=_YEbGAXCcAMC

[39] Mini-Circuits. (2015). *Stabilizing Network Technical Note*. [Online]. Available: https://www.minicircuits.com/app/AN60-064.pdf

[40] Keysight Technologies. (2020). *Noise Figure Measurement Accuracy: The Y-Factor Method*. [Online]. Available: https://www.keysight.com/us/en/assets/7018-06829/application-notes/5952-3706.pdf

GOKHAN ARITURK (Graduate Student Member, IEEE) received the B.Sc. and M.Sc. degrees in electrical and electronics engineering from Bilkent University, Ankara, Turkey, in 2015 and 2018, respectively. He is currently pursuing the Ph.D. degree with the Advanced Radar Research Center (ARRC), The University of Oklahoma, Norman, OK, USA.

From 2015 to 2018, he worked as a Graduate Research Assistant with the Electromagnetic Tissue Properties Laboratory, Bilkent University, conducting research in RF hardware for high-field MRI transceivers. He also worked on computational electromagnetics algorithms for MRI based electrical tissue properties mapping (MR-EPT) with Bilkent University. From the spring of 2018 to 2019, he worked as an RF Engineer with Turkish Aerospace Industries (TAI), Ankara, where he participated in the design and modeling of antennas for airborne radar systems. He is conducting research on the design of lossy and active microwave filters for integrated microwave transceivers. He is also working on the design of SIW based tunable filters for integrated phased array antenna systems.

HJALTI H. SIGMARSSON (Senior Member, IEEE) received the B.Sc. degree in electrical and computer engineering from the University of Iceland, Reykjavik, Iceland, in 2003, and the M.Sc. and Ph.D. degrees in electrical and computer engineering from Purdue University, West Lafayette, IN, USA, in 2005 and 2010, respectively.

He is currently with the School of Electrical and Computer Engineering and the Advanced Radar Research Center (ARRC), The University of Oklahoma, Norman, OK, USA, where he is an Associate Professor. His current research is focused on reconfigurable RF and microwave hardware for agile communications, measurement, and radar systems. His research interests include spectral management schemes for cognitive radio architectures, advanced packaging utilizing heterogeneous integration techniques, and additive manufacturing of electromagnetic components.

Dr. Sigmarsson was a recipient of the Best Paper Award from the IMAPS 2008 41st International Symposium on Microelectronics. In 2015, he was awarded the Air Force Office of Scientific Research (AFOSR) Young Investigator Program (YIP) to support his research on reconfigurable high-frequency components using phase-change materials. He was named a recipient of the Gerald Tuma Presidential Professorship in 2018 for meeting the highest standards of excellence in scholarship and teaching.

• • •